STRUCTURE OF HYDROGEN COMPRESSION PLASMA FLOWS IN A MAGNETOPLASMA COMPRESSOR

S. I. Ananin

UDC 533.95

Introduction. This paper is a continuation of [1-5], which dealt with the dynamics of compression plasma flows (CPFs) in magnetoplasma compressors (MPCs). Air CPFs were considered in [1, 3]. A two-dimensional model was proposed for describing the dynamics and structure of partially ionized radiating CPFs. The model was based on the coarse-particle method, introducing a magnetic field [6] and taking energy transfer by radiation into account within the framework of the two-flow multigroup approximation [7]. Calculations with this model determined the dynamics and structure of discharge in air and its principal radiative characteristics. Inclusion of the radiation has been shown to have a substantial effect on the plasma parameters in the compression region, considerably increasing the degree of plasma compression and lowering its temperature. In [2, 4, 5] this approach was used to describe the dynamics and structure of hydrogen CPFs. The work on the computational modeling of CPFs was started by Brushlinskii and Morozov [8]; the first studies considered hydrogen plasma (fully ionized). Those studies determined the qualitative features of the behavior of a CPF in an MPC. The dynamics of hydrogen CPFs with allowance for ionization was studied in [8-10]. This was done by using the approximation of discontinuous complete ionization of a plasma upon passage through a certain temperature T* [8, 9] or the modeling was done with detailed calculation of ionization from the Saha equation, but in the quasi-one-dimensional approximation [10]. The radiation of the plasma was not taken into account. The first calculations from two-dimensional models of hydrogen CPFs with allowance for the partial ionization and energy transfer by radiation were described in [2, 4, 5]. The dynamics and structure of hydrogen CPFs, generated by MPCs at low (20-100 kA) currents were calculated in [4]. The effect of boundary conditions on the results of computational modeling were considered in [5], where good agreement between theoretical and experimental results was demonstrated. Here we have studied the dynamics and structure of a CPF in the general case (without restrictions on the current) for the operation of an MPC under various conditions. Fairly extensive experimental data have been accumulated to date on the processes in an MPC. The most complete experimental results on hydrogen CPFs were published in series of studies [11-14], [2, 15-17], and [18, 25]. The results of computational modeling for the conditions of [2, 15-17] were described in [2, 4, 5] and this paper considered the modes and conditions under which the first experiments [11-14] were carried out and which are characterized by high discharge currents. A more detailed exposition of the development of work on computational modeling of gas as CPFs and references to studies on the calculations of erosion plasma flows can be found in the reviews [8, 19, 20] and in [3-5].

The present paper also discusses problems associated with the formation of current loops. Current loops (sometimes also called "current vortices") in coaxial accelerators were first discovered in the calculations of Brushlinskii, Gerlakh, and Morozov [21]. Some conditions of the formation of current loops were analyzed in [22, 23] in an analytical approximation with the picture substantially simplified. The existence of such loops was later also recorded experimentally [24, 25]. The effect of the current structure on the parameters and structure of the compression region is considered here as one topic. In [26] it was shown experimentally that under certain conditions the compression region in a gas MPC is "tubular," i.e., the region of maximum electron density is shifted relative to the axis of the system and we demonstrate here that this phenomenon is associated with the structure of current distribution.

Description of the Model. The system of nonstationary equations of magnetic radiation gasdynamics, describing the processses under discussion, looks as follows (the temperatures of ions, electrons, and atoms as well as their velocities, are assumed to be identical:

$$T_i = T_e = T_a = T,\ \mathbf{w}_i = \mathbf{w}_e = \mathbf{w}_a = \mathbf{w})$$

Minsk. Translated from Zhurnal Prikladnoi Mekhaniki i Tekhnicheskoi Fiziki, No. 4, pp. 3-9, July-August, 1991. Original article submitted February 26, 1990.

0021-8944/91/3204-0465$12.50

$$\frac{\partial \rho}{\partial t} + \operatorname{div}(\rho \mathbf{w}) = 0, \quad \frac{\partial \rho v}{\partial t} + \operatorname{div}(\rho v \mathbf{w}) + \frac{\partial p}{\partial r} + \frac{H}{4\pi r}\frac{\partial}{\partial r}(rH) = 0,$$

$$\frac{\partial \rho u}{\partial t} + \operatorname{div}(\rho u \mathbf{w}) + \frac{\partial p}{\partial z} + \frac{H}{4\pi}\frac{\partial H}{\partial z} = 0,$$

$$\frac{\partial \rho E}{\partial t} + \operatorname{div}((p + \rho E)\mathbf{w} + \mathbf{S}) + \frac{H}{4\pi}\left(\frac{v}{r}\frac{\partial rH}{\partial r} + u\frac{\partial H}{\partial z}\right) - \frac{\lambda}{4\pi}\left[\frac{1}{r^2}\left(\frac{\partial}{\partial r}rH\right)^2 + \left(\frac{\partial H}{\partial z}\right)^2\right] = 0,$$

$$\frac{\partial H}{\partial t} = \frac{\partial}{\partial r}\left[\frac{\lambda}{r}\frac{\partial}{\partial r}(rH)\right] + \frac{\partial}{\partial z}\left(\lambda\frac{\partial H}{\partial z}\right) - \frac{\partial}{\partial r}(vH) - \frac{\partial}{\partial z}(uH),$$

$$p = p(\varepsilon, \rho), \; E = \mathbf{w}^2/2 + \varepsilon.$$

Here ρ is the plasma density; p is the pressure; w is the velocity ($u = w_z$, $v = w_r$); ε is the specific internal energy; S is the energy flux due to radiation; $\lambda = c^2/(4\pi\sigma_e)$; and σ_e is the conductivity.

The energy transfer by radiation was calculated by the method proposed in [27]. The radiation fluxes in this case were considered in the multigroup two-flow approximation in the coordinates r and z. In the given case the spectral composition of the radiation was taken into account in the approximation of three spectral groups. Inside each group the absorption coefficients were assumed to be independent of the frequency and equal to that averaged over the Planck distribution within the given group. The boundaries of the intervals were 0.01-10.2; 10.2-13.6; 13.6-250 eV. The absorption coefficients for the respective spectral groups include the absorption in lines, bremsstrahlung and photoabsorption. In computational modeling these coefficients were determined by interpolation between the entries in previously calculated tables of values. The procedure for calculating the absorption coefficients was described in [28]. We prescribed the equations of state in two ways in order to determine the pressure and temperature from the values of the density ρ and the specific internal energy ε: 1) by interpolation, as for the absorption coefficients; the equations of state were tabulated, using the data of [29]; 2) direct calculation of the ionization composition of the plasma on the assumption that there exists local thermodynamic equilibrium according to the Saha equation. In the latter case we used the expression $\varepsilon = (1 + \alpha)c_V T + \zeta\alpha I_1/m_i$ (α is the degree of ionization, I_1 is the ionization potential, and m_i is the ion mass). The coefficient ζ characterizes the "ion value." For the plasma pressure we have $p = (1 + \alpha)(c_p - c_V)\rho T$. At $\zeta = 1$ the second way of prescribing the equations of state is equivalent to the first and by assigning $\zeta > 1$ we can effectively take account of the radiation loss during ionization, which may exceed the values corresponding to local thermodynamic equilibrium [10].

The radiation was taken into account in a simpler way for a low-density plasma: from the formulas for bremsstrahlung and recombination radiation [30], which are applicable to a plasma with a low optical density, when deexcitation is a volume process. It thus becomes possible to take impurities in the working gas into account approximately by introducing the effective charge Z. Special test calculations were carried out to check the equivalence of the treatments for determining the radiation fluxes in the multigroup two-flow approximation and in the volume deexcitation approximation (naturally, at the same plasma densities and temperatures for which the conditions of volume deexcitation are satisfied).

The method used here to set the boundary conditions does not differ from that described in [4, 5]. Initially, the calculated region (its geometry is taken from the corresponding experiment) is assumed to be filled with a hydrogen plasma of density ρ_0 and temperature T_0 and the magnetic field is zero.

A net with 40 × 60 cells was customarily used in the calculations. The scheme for dividing the region into whole and fractional cells is shown in Fig. 1 in [1]. Some details concerning the finite-difference scheme of the model can be found in [7] and in the references given there.

Results of Calculations. We consider the results of computational modeling under the following conditions: $T_0 = 11.6$ kK, $\rho_0 = 5.9 \cdot 10^{-4}$ kg/m^3 (this density at normal temperature corresponds to $p_0 = 667$ Pa), $\zeta = 2$, and $u_s = 3 \cdot 10^3$ m/sec. The oscilloscope trace of the total discharge charge [the dependence $I_p(t)$] used in the calculations was obtained by linear interpolation of the values of the current given in Fig. 15 of [12] and the geometry of the discharge device corresponds to that shown in Fig. 6b of [12].

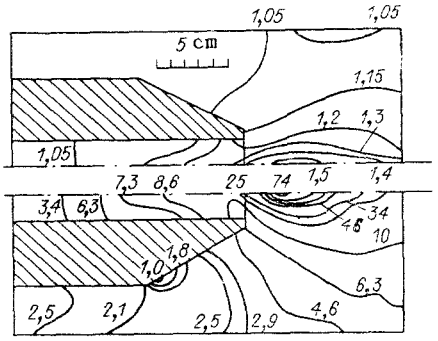

Fig. 1

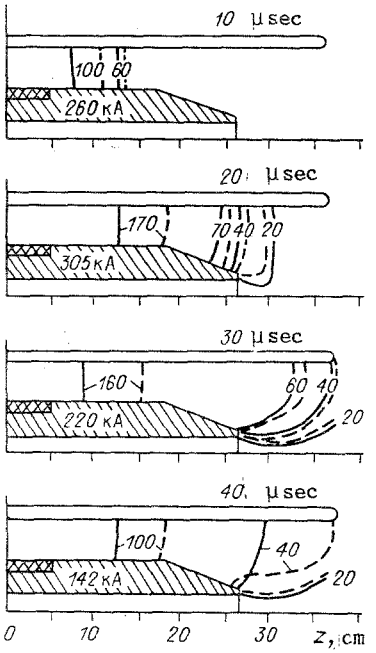

Fig. 2

The results of calculations show that when current begins to flow in the interelectrode gap a shock wave, sometimes called a prebunch, is formed; moving along the electrodes, at roughly 20 μsec (I_p = 305 kA) it reaches the end of the central electrode and a compression region begins to form on the axis of the system. At approximately 25 μsec the prebunch leaves the limits of the computational region and the plasma velocity at the generating cone of the central electrode reaches $3 \cdot 10^4$ m/sec. Figure 1 shows the distributions of the temperature (upper half-plane) and electron density at t = 30 μsec. The unit of temperature on the isotherms is 11.6 kK and the unit of density on the isopycnic line is 10^{22} m^{-3}. The total discharge current at the given time is 220 kA.

A compression region with a diameter (at the level of half the maximum density) ~1 cm and length ~9 cm is visible on the axis of the system. The plasma temperature in the compression region reaches 17 kK and the electron density reaches $n_e \approx 7 \cdot 10^{23}$ m^{-3}. The axial-flow velocity of the plasma in the vicinity of the central electrode is $\sim 2 \cdot 10^4$ m/sec. The velocity field has a complex structure in the vicinity of the exit cross section of the diverter: A considerable part of the cathode plasma flows into the diverter in the direction counter to the main flow. The diverter is filled with plasma at a speed which reaches $\sim 10^4$ m/sec at t = 30 μsec (in the entrance cross section of the diverter). By 40 μsec the total discharge current drops to 142 kA but the general structure of the CPF changes only slightly in the computational region. The radius and length of the compression region increases 1.5 times. The maximum temperature decreases to 16 kK and the maximum density decreases to $3 \cdot 10^{23}$ m^{-3}. The pressure at the left end of the diverter* increases so much by this time that the plasma begins to flow away in the direction of the main flow, although the flow into the diverter continuesin the entrance cross section. By ~50 μsec the diverter "loses control" almost entirely and plasma begins to flow out of the diverter through the entrance cross section (apart from a small paraxial zone, where flow into the diverter continues because of the plasma pressure in the compression region).

The current distribution in the MPC was measured with magnetic probes in [12]. Figure 2 shows the distributions obtained in these experiments (solid lines) and by compuational modeling (dashed lines). The unit of current on the isolines is 1 kA. The theoretical and experimental data are in good agreement. It is particularly favorable that the data obtained for the outflow currents beyond the end of the cathode in the vicinity of the compression region are close. Since the electromagnetic fields are the "skeleton," as it were, of the entire CPF structure, we can hope for agreement between other CPF parameters, at least in the compression region. The results of a comprehensive study for other parameters (distribu-

*Here we consider the geometry of a central electrode with a "dead-end" diverter, i.e., the diverter opening at z = 0 ends with a wall.

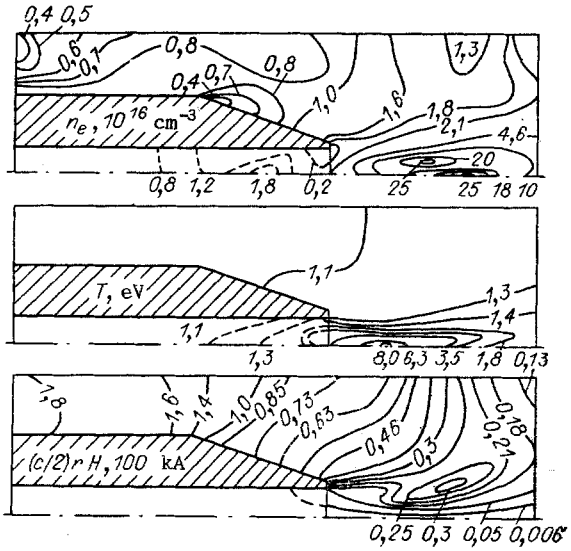

Fig. 3

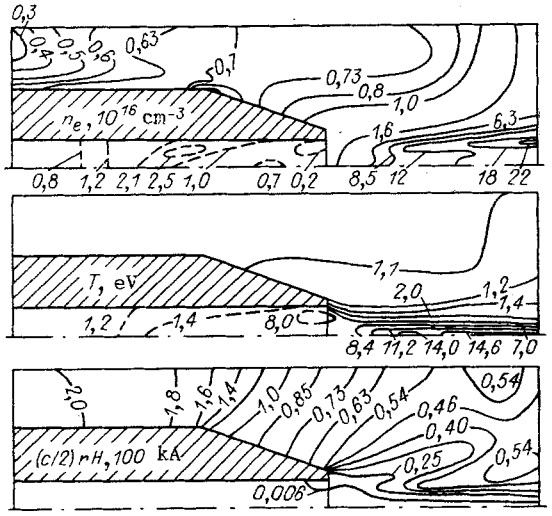

Fig. 4

tions of n_e, T_e, etc.) under the same conditions were not published in [12], however. The results of measurements of n_e and T in a device with the same geometry are given in [14] for different conditions (p_0 = 40 Pa). In order to compare these data with theoretical data we carried out calculations at T_0 = 11,600 K, $p_0 = 3.54 \cdot 10^{-5}$ kg/m^3 (this density corresponds to p_0 = 40 Pa at normal temperature), $u_s = 8 \cdot 10^3$ m/sec, and ζ = 2, using the oscilloscope trace of $I_p(t)$ obtained by linear interpolation of the values of the current given in Fig. 8 of [11]. In this case was calculated in the volume deexcitation approximation without allowance for radiation transfer. The geometry of the discharge device was assumed to be the same as in the preceding calculation.

Since the initial pressure in the chamber varied by more than an order of magnitude the conditions of the given discharge differ substantially from those described above. The passage of the plug accelerates (passage time ~18 μsec) and the plasma temperature rises rapidly in the compression region. The maximum plasma temperature on the axis of the system reaches 35 kK at 22 μsec and 93 kK at 26 μsec. At t = 30 μsec, when I_p = 205 kA, the maximum velocity at the end of the electrode is $1 \cdot 10^5$ m/sec (at p_0 = 667 Pa it is ~$2 \cdot 10^4$ m/sec, although the total discharge current is lower at p_0 = 40 Pa). The changes affected the very structure of the compression region. Figure 3 shows (top and bottom) the distributions of the electron density, the plasma temperature, and the currents (unit of density 10^{22} m^{-3}, unit of temperature 11,600 K, unit of current 100 kA) at t = 26 μsec. At this time the elec-

TABLE 1

n_e^{max}, m^{-3}	T^{max}, kK	Length of compression region, cm
Experiment [14]		
$(2,8\pm0,3)\cdot10^{23}$	130±23	6
Computational modeling at $t = 26$ μsec		
$2,5\cdot10^{23}$	93	9
at $t = 30$ μsec		
$2,2\cdot10^{23}$	170	≥20

tron-density distribution has two maxima in the compression region. One of them is on the discharge axis, as before, and the other is 1 cm from the axis. A zone with higher values of n_e than at the axis thus exists on the periphery of the compression region. This structure is sometimes called "tubular" (its existence in an MPC was reported in [26]). A distinctive feature also appeared in the distribution of the current (to be more precise, in the distribution of crH/2): The maximum of the toroid formed beyond the cathode end and its position correlates with the position of the nonaxial maximum in the electron-density distribution. As the flow velocity continues to grow this maximum moves away from the central electrode. At t = 30 μsec, n_e at the nonaxial maximum is almost double the value on the axis, reaching $2\cdot10^{23}$ m^{-3} (Fig. 4). The plasma-temperature distribution in the compression region also becomes complicated. It remains uniform along the radius, i.e., with one axial maximum, and a second maximum on the axis arises in the plasma-temperature distribution. The temperatures at both maxima are similar, amounting to 160-170 K.

Before going directly to a comparison of the results of computational modeling and experiments, we note some complexities that arise. First, the processes under consideration are essentially unsteady. Since the breakdown stage is not described in the model, we must make allowance for a possible time shift relative to the experimental reading (even forgetting about some time spread of the delays in the experiment). Second, although it is macrostable, an actual compression flow executes transverse vibrations about the axis of the system, whose amplitude in the compression region reaches 1 cm [14], i.e., there is no complete symmetry about the axis of the system. This imposes some a priori limitations on the attainable degree of correspondence between theory and experiment, especially if the experimental data are obtained by averaging over several discharges, when a "fine structure" of the type depicted in Figs. 3 and 4 will be smeared, as it were, because of averaging.

The results of measurements of T and n_e by photoelectric recording of the continuum were given in [14]. Radial distributions of T and n_e at t = 30 μsec were obtained for z = 3 and 6 cm, respectively (Figs. 2 and 3 of [14]). The radial distribuitons cf the temperature are characterized by one maximum (at r = 0) and a monotonic decrease with distance from the axis of the system while in addition to the axial maximum the electron-density distribution has a small maximum at r ~ 4 cm ($n_e \approx 6\cdot10^{22}$ m^{-3} and at r = 3 and 4.4 cm for z = 6 cm, $n_e \approx 4\cdot10^{22}$ m^{-3}). Most of the distinctive features of the distributions of T and n_e [the values at the maxima, the existence of two maxima in the distributions $n_e(r)$ and one in the T(r) distributions] accord well with the distinctive features of the temperature and plasma-density distributions given in Figs. 3 and 4 (see Table 1). As we see from Table 1, the best agreement between the experimental data and the results of computational modeling is observed for t = 26 μsec, which is natural according to the above suggestions that the computational time somewhat "leads" the real time because the model does not make allowance for the breakdown stage and the initial plasma formation. The substantial overestimation of the length of the compression region during modeling is attributable to the fact that the experimentally detected nonaxisymmetric variations do not appear in a real plasma flow.

The results of Michelson interferometer measurements of the distribution of n_e in the same discharge device, but for a slightly different initial pressure p_0 = 33 Pa, were described in [11]. Averaging of these results over many discharges gave the patterns of the two-dimensional distribution of n_e in the compression region (Fig. 8, [11]). Comparison of the experimental distributions for t = 30 μsec and the corresponding distributions in Fig. 3 also reveals considerable agreement. The maximum experimental value of n_e was $2\cdot10^{23}$ m^{-3}

(±30%), the length of the compression region was 6 cm, and the $n_e = 4 \cdot 10^{22}$ m^{-3} isoline in the compression region is almost horizontal with r ≈ 1 cm. In the n_e distribution obtained by computational modeling this radius is also twice as large, i.e., with respect to radius as well the width of the experimental n_e distribution is larger than that predicted by computational modeling. The fact that the experimental distribution $n_e(r)$ does not have a second maximum in the compression region is one of the major differences. We must note, however, that the pattern of Fig. 8 of [11] is an integrated pattern and also that under similar conditions such a second maximum was recorded experimentally (Fig. 3, [14]), when the distribution was taken in one discharge.

In summary, the calculations have shown that the proposed model can describe all the formative stages and the dynamics of a compression plasma flows, apart from breakdown. It has been demonstrated that under certain conditions the compression region takes on a "tubular" structure (with respect to n_e), as discovered earlier in experiments [26]. Under these conditions the current structure is characterized by the presence of current loops near the compression region. The results of modeling are in good agreement with the experimental findings on the magnetic field distribution (experiments [12]) and the plasma-temperature distribution [14]. The available experimental data on the electron-density distribution are insufficient to make a conclusion about the degree of agreement with the results of computational modeling, in particular, to definitely solve the problem of the existence of a "tubular" structure under the specific experimental conditions [11, 14]. The compresion region determined in the experiments is larger than that found from the modeling data. The maximum densities in the compression region, however, virtually coincide (see Table 1). On the whole, comparison of the results of computational modeling and experiments [11, 12, 14] indicate that our model is fairly adequate. Bearing in mind that such conclusions were made on the basis of comparison with experimental data [2, 15-17], obtained on a different magnetoplasma compressor under different conditions, we can conclude that this model is suitable for use to optimize MPC design and to choose the conditions for CPF generation.

LITERATURE CITED

1. S. I. Ananin, "Calculation of the dynamics of compression plasma flows in an air magnetoplasma compressor," Teplofiz. Vys. Temp., 23, No. 5, (1985).
2. L. Ya. Min'ko, S. I. Ananin, V. M. Astashinsky, et al., "Dynamics of low-energy compression plasma flows," Proceedings of the 17th Int. Conf. on Phenomena in Ionized Gases, Vol. 2, Budapest (1985).
3. S. I. Ananin, "Dynamics of plasma flows in a gas magnetoplasma compressor," Teplofiz. Vys. Temp., 24, No. 6 (1986).
4. S. I. Ananin and L. Ya. Min'ko, "Computational modeling of compression plasma flows generated by a gas magnetoplasma compressor at low (20-100 kA) currents," Izv. Akad. Nauk BelorusSSR, Ser. Fiz.-Mat. Nauk, No. 5 (1986).
5. S. I. Ananin and L. Ya. Min'ko, "Structure and parameters of radiating compression plasma flows calculated with allowance for configuration of plasma-forming channel," Fiz. Plazmy, 15, No. 8 (1989).
6. S. I. Ananin and T. A. Lepshei, "Computational modeling of the dynamics of compression plasma flows by the coarse-particle method," Dokl. Akad. Nauk BelorusSSR, 27, No. 8 (1983).
7. S. I. Ananin and T. A. Lepshei, "Formation and dynamics of radiating plasma flows in a magnetoplasma compressor," Preprint No. 325 [in Russian], Physics Institute, Academy of Sciences, Belorussian SSR, Minsk (1984).
8. K. V. Brushlinskii and A. I. Morozov, "Calculation of two-dimensional plasma flows in channels," in: Vopr. Teor. Plazmy, Vol. 8 [in Russian], Atomizdat, Moscow (1974).
9. V. V. Savel'ev, "Two-dimensional calculation of the flow of an ionizing gas in an accelerator channel," Pis'ma Zh. Tekh. Fiz., 2, No. 13 (1976).
10. K. V. Brushlinskii, G. A. Kalugin, and A. N. Kozlov, "Computational modeling of ionizing gas in a channel," Preprint No. 50 [in Russian], Institute of Mechanics, Academy of Sciences of the USSR, Moscow (1982).
11. V. I. Berkov, A. K. Vinogradova, P. E. Kovrov, et al., "Estimation of the parameters of a plasma in the accelerating channel and the compression zone of a MPC," Preprint No. 2267 [in Russian], I. V. Kurchatov Institute of Atomic Energy, Moscow (1973).
12. V. I. Berkov, A. K. Vinogradova, P. E. Kovrov, et al., "Experimental study of flow in a MPC," Preprint No. 2275 [in Russian], I. V. Kurchatov Institute of Atomic Energy, Moscow (1973).

13. A. K. Vinogradova and A. I. Morozov, "Steady-state compression flows," in: Physics and Applications of Plasma Accelerators [in Russian], Nauki i Tekhnika, Minsk (1974).
14. V. I. Berkov and A. I. Morozov, "Plasma parameters in the compression zone of a magnetoplasma compressor," Pis'ma Zh. Éksp. Teor. Fiz., 19, No. 1 (1974).
15. L. Ya. Min'ko, V. M. Astashinskii, G. I. Bakanovich, et al., "Pulsed plasma accelerator based on the discharge device of a compact magnetoplasma compressor," Izv. Akad. Nauk BelorusSSR, Ser. Fiz.-Mat. Nauk, No. 2 (1968).
16. L. Ya. Min'ko, S. I. Ananin, V. M. Astashinskii, et al., "Experimental study and computational modeling of the physical processes in a compact MPC," in: Plasma Accelerators and Ion Injectors [in Russian], Izd. Dnepropetrovsk. Univ., Dnepropetrovsk (1986).
17. L. Ya. Min'ko, S. I. Ananin, V. M. Astashinskii, et al., "Dynamics of radiating compression plasma flows," in: Proceedings of the 6th All-Union Conference on the Dynamics of a Radiating Gas [in Russian], Moscow (1987).
18. K. V. Brushlinskii, A. N. Kozlov, S. A. Trubchaninov, and V. I. Voznyi, "Comparative analysis of the characteristics of a small MPC with solid electrodes," in: Plasma Accelerators and Ion Injectors [in Russian], Izd. Dnepropetrovsk. Univ., Dnepropetrovsk (1986).
19. N. V. Ardelyan, K. V. Kosmachevskii, N. P. Kozlov, et al., "Computational modeling and theoretical study of radiating plasmadynamic discharges," in: Proceedings of the 1st All-Union Symposium on Radiation Plasma Dynamics [in Russian], Énergoatomizdat, Moscow (1989).
20. K. V. Brushlinskii, "Computational modeling of ionizing gas flows in channels," in: Plasma Accelerators and Ion Injectors [in Russian], Nauka, Moscow (1984).
21. K. V. Brushlinskii, N. I. Gerlakh, and A. I. Morozov, "Two-dimensional steady-state flow of a highly conducting plasma in a coaxial system," Izv. Akad. Nauk SSSR. Mekh. Zhidk. Gaza, No. 2 (1966).
22. L. M. Alekseeva and L. S. Solov'ev, "Current vortices and critical surfaces in a magnetohydrodynamic flow," Prikl. Mat. Mekh., 28 (1964).
23. A. I. Morozov and L. S. Solov'ev, "Steady-state plasma flows in a magnetic field," Problems of Plasma Theory [in Russian], Vol. 8, Atomizdat, Moscow (1974).
24. A. K. Vinogradova, P. E. Kovrov, A. I. Morozov, et al., "General pattern of plasma flow in a magnetoplasma compressor," Zh. Tekh. Fiz., 43, No. 12 (1973).
25. I. E. Garkusha, A. V. Zolotukhin, O. E. Kazakov, et al., "Character of the current distribution in the rod cathode of a MPC," in: Plasma Accelerators and Ion Injectors [in Russian], Izd. Dnepropetrovsk. Univ., Dnepropetrovsk (1986).
26. L. Ya. Min'ko, V. M. Astashinskii, and E. A. Kostyukevich, "Dynamics of the formation and decay of a compression plasma flow," Teplofiz. Vys. Temp., 25, No. 3 (1987).
27. M. A. El'yashevich, G. S. Romanov, and Yu. A. Stankevich, "Calculation of the parameters of light-erosion plasma flames with allowance for the spectral dependence of their radiative characteristics," in: Proceedings of the 4th All-Union Conference on the Dynamics of a Radiating Gas [in Russian], Vol. 1, Izd. Mosk. Gos. Univ., Moscow (1981).
28. F. N. Borovik, S. I. Kas'kova, G. S. Romanov, et al., "Optical properties of bismuth plasmas," Zh. Prikl. Spektrosk., 39, No. 6 (1983).
29. V. P. Kopyshev and V. V. Khrustalev, "Hydrogen equations of state up to 10 Mbar," Prikl. Mekh. Tekh. Fiz., No. 1 (1980).
30. Ya. B. Zel'dovich and Yu. P. Raizer, Physics of Shock Waves and High-Temperature Hydrodynamic Phenomena [in Russian], Nauka, Moscow (1966).